JOURNAL OF MATERIALS SCIENCE **40** (2005) 1943–1952

# Computational analysis of the lattice contribution to thermal conductivity of single-walled carbon nanotubes

M. GRUJICIC*, G. CAO
*Department of Mechanical Engineering, Program in Materials Science and Engineering, Clemson University, Clemson SC 29634*
*E-mail: mica.grujicic@ces.clemson.edu*

WALTER N. ROY
*Army Research Laboratory—WMRD AMSRL-WM-MD, Aberdeen, Proving Ground, MD 21005-5069*

Molecular dynamics based heat-flux auto-correlation functions are combined with a Green-Kubo relation from the linear response theory to quantify the lattice contribution to thermal conductivity of single-walled carbon nanotubes with three different chiralities (screw symmetries). The interactions between carbon atoms within a nanotube are analyzed using the Adaptive Intermolecular Reactive Empirical Bond Order (AIREBO) potential. The results obtained show that, due to a long-term exponential-decay character of the heat-flux auto-correlation functions, converging values of the lattice thermal conductivities can be obtained using computational cells considerably smaller than the phonon mean free path. However, to obtain accurate values of the thermal conductivity, a spectral Green-Kubo relation and a phonon-based extrapolation function are found to be instrumental for quantifying the thermal conductivity contribution of the long-wavelength phonons not allowed in the computational cells of a finite size. The results further show that chirality of the carbon nanotubes can affect the lattice contribution to the thermal conductivity by as much as 20%. Also, the simulation results of the effect of temperature on the thermal conductivity clearly show a competition between an increase in the number of phonons and an increased probability for phonon scattering at higher temperatures.


## 1. Introduction

As the size of electronic, optical and mechanical devices is being constantly reduced and the speed of their operation is being steadily increased, the thermal conductivity of materials at the micro/nano length scale is becoming an increasingly important issue since for a reliable operation of such devices, significant amounts of heat may need to be dissipated from relatively small regions. In general, however, experimental determination of the thermal conductivity in nano-scale devices is quite difficult [e.g. 1], particular in the case of devices with complex geometries. Hence, the development of reliable theoretical and computational methods for predicting thermal properties of the materials and the devices at a micro/nano length scale is of an utmost importance [e.g. 2].

Because of their unique properties (e.g. high hardness and stiffness, light weight, tailorable electronic and optical properties, high chemical stability, etc.), carbon nanotubes are being currently explored as prime candidate materials in nano-scale device applications. Hence, considerable effort has been invested in characterizing properties of carbon nanotubes, particularly their electronic and mechanical properties [3–6]. Recently, similar attention has been devoted to the understanding of thermal properties of carbon nanotubes, since they are being considered for thermal management in nano-scale devices. As mentioned above, substantial challenges are associated with nano-scale experimental measurements of the thermal conductivity. These difficulties are further compounded by major technological challenges associated with synthesizing high-quality, well-ordered nanotubes suitable for experimental measurements. Hence, analytical and numerical calculations of the thermal conductivity of carbon nanotubes are presently considered as essential tools for elucidating the mechanism and for quantifying the effectiveness of heat transport in these materials.

Theoretical calculations of the thermal conductivity of materials can be generally classified into two main

*Author to whom all correspondence should be addressed.

categories: (a) First principles based atomistic simulations [e.g. 7–9]. This approach is particularly useful for nano-scale devices where an experimental determination of the thermal conductivity is quite challenging; and (b) Continuum calculations based on transport theories such as the Boltzmann transport equation [10–12]. The main advantage of the continuum approach is that it enables an analysis of relatively large systems. However, the approach entails the knowledge of certain materials parameters such as the phonon relaxation time and the phonon density of states which must be determined using either experimental measurements (also associated with major difficulties in the case of nano-scale devices) or by theoretical calculations (can be quite challenging, time consuming, and/or of a questionable accuracy). An additional shortcoming of the continuum approach is that the governing integro-differential transport equation may be difficult to solve for some device geometries and boundary conditions.

Due to the aforementioned limitations of the continuum approach, the first principles based atomistic simulations are beginning to receive increasingly more attention as a means of computing the thermal properties of materials at the nano length scale. In addition to not requiring a prior knowledge of the model parameters, atomic-scale calculations enable quantification of the effect of microstructure (e.g. phase interfaces and surface reconstruction) on thermal properties. In situations in which the device is too large for its thermal properties to be studied using an atomic-scale approach, atomistic simulations can be used to determine the parameters needed by the continuum models, as discussed above. Thus, in the latter case, atomistic simulations can be used to help bridge the gap between the atomistic-scale and the continuum-level calculations.

Thermal conductivity of a material generally includes two main components: (a) an electronic component which is controlled by the electronic band structure, electron scattering, and electron-phonon (lattice vibrations) interaction; and (b) a lattice component which is mainly controlled by the motion of phonons and phonon scattering. In the present paper, only the lattice contribution to thermal conductivity of carbon nanotubes is considered using atomistic simulations. It should be noted that the electronic contribution to thermal conductivity is very small and can be neglected in materials with relatively large band gaps. As far as the carbon nanotubes are concerned, the size of their band gap is found to be dependent on their chirality (screw symmetry), as well as on their diameter and length. The largest band gap (on the order of 1.5 eV) is found in small diameter, short $(n, m)$ nanotubes with the rollup vectors $n$ and $m$ satisfying the condition: $|n-m| \neq 3p$, where $p$ is an integer. For other types of nanotubes, the band gap is considerably smaller and tends to approach zero in the case of "arm chair" nanotubes in which $n = m$. For comparison, the band gap in a typical insulator is on the order of 5–10 eV, of a semiconductor in a range between 0.5–2.5 eV, and zero in a typical metal. Based on these observations, one may anticipate that the electronic contribution to thermal conductivity in carbon nanotubes, can be significant only in the case of carbon nanotubes with a small band gap, i.e., in the nanotubes which exhibit a metallic-type behavior.

When thermal conductivity of solid crystalline materials is being calculated using an atomic-scale approach, one may expect that the size of the computational cell must be at least as large as the mean free path of the phonons in order to prevent phonon scattering from the cell boundaries. This may pose a serious computational challenge since the phonon mean free path can be on the order of hundreds of nanometers and, hence the computational domain may have to contain hundreds of thousands of atoms. In addition, quantification of phonon-phonon interactions (responsible for the finite values of thermal conductivity) is generally very complicated [e.g. 13]. In a recent study, Che *et al*. [2] carried out molecular dynamics simulations and used the linear-response theory based Green-Kubo equation and the energy-flux auto-correlation functions to determine the thermal conductivity of diamond. They found that while the accuracy of the thermal conductivity is indeed dependent on the size of the periodic cell, an accurate thermal conductivity can be obtained using periodic computational cells whose edge lengths are about 40–60 times smaller than the actual phonon mean free path. They attribute this finding to the fact that the heat-flux auto-correlation time is much shorter than the energy relaxation time. The approach of Che *et al*. [2] was used in our recent work [14] to determine the lattice contribution to the thermal conductivity of single-walled carbon nanotubes at different temperatures. The results obtained suggested that the values of lattice thermal conductivity tend to converge with an increase in the computational cell size at the cell sizes which are substantially smaller than the average phonon mean free path in these materials. In the present paper, we extend our previous work [14] in order to account for the contribution of long-wavelength phonons to the lattice thermal conductivity. Such phonons are not permitted in the computational cells typically used in molecular dynamics simulations. On the other hand, such phonons may have a significant contribution to the lattice thermal conductivity.

The organization of the paper is as follows: A brief overview of the theoretical background related to the computation of thermal conductivity and the details of the computational method used are given in Sections 2.1 and 2.2. The main results obtained in the present work are presented and discussed in Section 3. The key conclusions resulting from the present work are given in Section 4.

## 2. Procedure

### 2.1. Theoretical background

For the macroscopic-level steady-state heat conduction, thermal conductivity, $\Lambda$, is defined by the Fourier's law as:

$$\vec{J}_{\mathrm{q}} = -\Lambda \cdot \nabla T \tag{1}$$

where $\vec{J}_q$ is the steady-state heat flux vector, $\Lambda$ the thermal conductivity second order tensor and $\nabla T$ the temperature gradient. A raised arrow is used in Equation 1 and throughout this paper to denote a vector quantity.

In general, the total energy flux, $\vec{J}_E$, includes the conduction heat flux, $\vec{J}_q$, and the diffusion energy flux, $\mu\vec{J}$, where $\vec{J}$ is the particle flux, and $\mu$ is the particle chemical potential. Thus, the following relation can be defined between the total energy flux and the heat flux [15]:

$$\vec{J}_q = \vec{J}_E - \mu\vec{J}. \tag{2}$$

In solids, (except perhaps at extremely high temperatures), the contribution of diffusion to the energy flux can be neglected and hence: $\vec{J}_q = \vec{J}_E$.

In a classical system consisting of the discrete particles, the energy density at a location $r$, $h(r)$, can be expressed as the site energy of a particle at that location and consequently, the heat flux can be defined as:

$$\vec{J}_q = \frac{1}{V}\frac{d}{dt}\sum_i \vec{r}_i h_i \tag{3}$$

where $V$ is the system volume, $\vec{r}$ the particle position vector, subscript $i$ is used to denote particle $i$ and $t$ is the time.

One approach for the determination of the thermal conductivity by atomistic simulations is to place the computational cell in contact with two reservoirs with different temperatures ($T_1$ and $T_2$) and to calculate the heat flux when the system reaches the steady state. However, due to small dimensions of the computational cell (typically 10–50 nm edge side), even a small temperature difference of 10 K across the system corresponds to a thermal gradient on the order of $10^8$ K/m. It is unlikely that the linear response theory (i.e., the linearity between the heat flux and the temperature gradient as defined in Equation 1) would hold under such an extreme thermal loading condition. Moreover, this temperature gradient maybe smaller than the thermal fluctuations in the system, making it difficult to obtain convergence of the simulation results within reasonable simulation times.

Due to the aforementioned shortcomings of the approach, the Green-Kubo fluctuation-dissipation theorem [16] from the linear response theory which provides a connection between the energy dissipation in an irreversible process (e.g. heat conduction in the presence of a temperature gradient) and the equilibrium system fluctuations (of the heat flux) is used in the present work. Within this approach, the thermal conductivity tensor can be expressed in terms of the heat-flux auto-correlation functions, $C_J^C(t)$, [16, 17] as:

$$\Lambda^C = \frac{V}{k_B T^2}\int_0^\infty dt\, C_J^C(t) \tag{4}$$

where $k_B$ is the Boltzmann's constant, $T$ temperature and the heat-flux auto-correlation function is defined as:

$$C_J^C(t) = \langle \vec{J}_q(t)\cdot\vec{J}_q(0)\rangle. \tag{5}$$

$C_J^C(t)$is obtained by phase (particles positions and momenta) space ($\Gamma$) averaging as:

$$\langle \vec{J}_q(t)\cdot\vec{J}_q(0)\rangle = \frac{\int d\Gamma \exp(-\beta H)\vec{J}_q(t)\cdot\vec{J}_q(0)}{\int d\Gamma \exp(-\beta H)} \tag{6}$$

where

$$H = \sum_i h_i. \tag{7}$$

Within the framework of molecular dynamics simulations, Equation 7 is evaluated as:

$$\langle \vec{J}(t)\cdot\vec{J}(0)\rangle = \frac{1}{N_{corr}}\sum_{N_{corr}} \vec{J}(t_0+t)\cdot\vec{J}(t_0) \tag{8}$$

where

$$t = N_t\Delta t, \quad 0 \le N_t \le N_{MD} \tag{9}$$

$$t_0 = N_0\Delta t, \quad 0 \le N_0 \le N_{MD} - N_t \tag{10}$$

and

$$N_{corr} = \mathrm{int}\left(N_{MD}/N_t\right), \tag{11}$$

where $t_0$ and $t$ are respectively the zero and the current correlation times, $\Delta t$ is the simulation time increment, $N_{MD}$ is the total number of molecular dynamic simulation steps, $N_0$ and $N_t$ are integers, and *int* denotes an operator which converts a real number into the closest smaller integer.

It should be noted that the analysis presented above is classical, i.e., no quantum effects are considered. In general, quantum effects are not critical when the temperature is significantly higher than the Debye temperature. While the Debye temperature of carbon nanotubes and its dependence on the nanotube chirality are not well established, this temperature is expected to be considerably higher than the room temperature considering the magnitudes of the Debye temperature in other structural forms of carbon (e.g. around 2000 K for graphite and 1850–2200 K for diamond). Using a quantum-physics based analysis, Che *et al.* [2] showed that in (hypothetical) purely-harmonic systems in which different phonon modes do not interact, quantum effects are negligible. In real systems, on the other hand, phonons are coupled and this anharmonicity is, in fact, responsible for a finite value of the phonon mean free path, and hence, for a finite value of the thermal conductivity. Fortunately, thermal conductivity in such systems is dominated by low-frequency (long wavelength) phonons, which are generally considered as being nearly classical. Hence, a lack of inclusion of the quantum corrections is generally considered as being not very critical when calculating the thermal conductivity of carbon

TABLE I Structural characteristics of the carbon nanotubes studied in the preset work

| Nanotube type $(n, m)$ | Nanotube radius (nm) | Unit cell length (nm) | Number of atoms per unit cell |
|---|---|---|---|
| (10, 10) | 1.351 | 0.2477 | 40 |
| (18, 0) | 1.404 | 0.4290 | 72 |
| (14, 6) | 1.387 | 3.8130 | 632 |

nanotubes. As far the effects of anharmonicity are concerned, they are important but they are generally accounted for when (classical) molecular dynamics simulations based on realistic interatomic potentials are carried out. Hence, it appears justified to use molecular dynamics simulations to quantify the thermal conductivity of carbon nanotubes, as is done in the present work.

## 2.2. Simulation procedure

Molecular dynamics simulations are conducted using computational cells which are of a finite size in one and infinitely long in the other two directions. The periodic boundary conditions are applied in the finite direction. Each cell contains a single $(n, m)$ nanotube with the nanotube axis aligned with the direction in which the cell is finite. The dimension of the cell in the nanotube direction is varied in order to accommodate nanotubes of different chirality and, also, to explore the effect of the cell size on thermal conductivity. Three types of carbon nanotubes are studied in the present work: (a) a (10, 10) armchair type nanotube; (b) a (18, 0) zig-zag type nanotube; and (c) a (14, 6) nanotube. The first nanotube is selected because it is frequently found in synthesized nanotube bundles, while the other two are selected on the basis that they have the diameter comparable to that of the (10, 10) nanotube. Other structural characteristics of the three nanotubes are given in Table I while the corresponding atomic arrangements are shown in Fig. 1a–c.

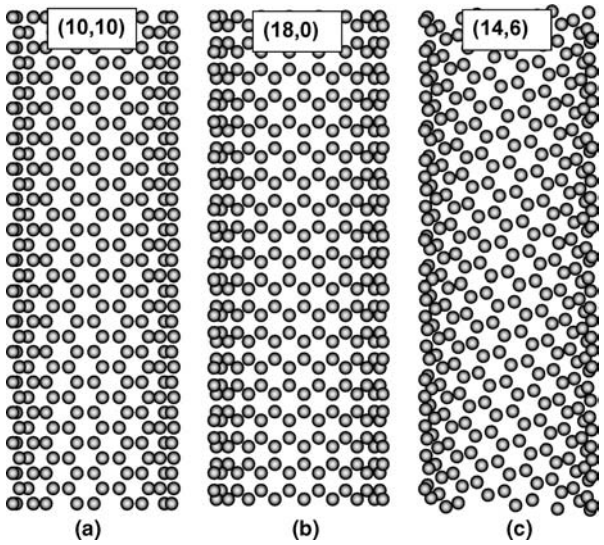


*Figure 1* Atomic Configuration associated with: (a) a (10, 10) arm-chair nanotube; (b) a (18, 0) zig-zag nanotube; and (c) a (14, 6) nanotube of a general chirality.

The interactions between carbon atoms have been modeled using the Adaptive Intermolecular Reactive Empirical Bond-Order (AIREBO) potential developed by Stuart *et al*. [18]. This potential is an extension of the original Brenner's Reactive Empirical Bond-Order (REBO) potential [19] and includes non-bonding (intermolecular) atomic interactions. It should be noted that while frequently the interactions between carbon atoms within a single single-walled carbon nanotubes are modeled using only the bonding part of an interatomic potential, the AIREBO potential used in the present work has been optimized to also include the non-bonding interactions between carbon atoms of the same single-walled carbon nanotube. Based on the AIREBO potential, the total potential energy, $V_{\text{tot}}$, can be approximately written as a summation of pair-wise and three-body interactions as [19]:

$$V_{\text{tot}} = \sum_i \sum_{j>i} V_{ij} + \sum_i \sum_{j>i} \sum_{k>j} V_{\text{ijk}}. \qquad (12)$$

where $V_{\text{ij}}$ and $V_{\text{ijk}}$ are respectively the two- and the three-body interaction potentials.

Consequently, the energy of site $i$, $h_i$, can be defined as:

$$h_{\text{i}} = \frac{p_{\text{i}}^2}{2m_{\text{i}}} + \frac{1}{2}\sum_{j\neq i} V_{\text{ij}} + \frac{1}{6}\sum_{j\neq i}\sum_{k\neq j, k\neq i} V_{\text{ijk}}. \qquad (13)$$

where $p_{\text{i}}$ and $m_{\text{i}}$ are respectively the momentum and the mass of atom $i$. Under the condition of a zero net momentum for the computational system, a combination of Equations 13 and 3 yields:

$$\vec{J}_{\text{q}}(t) = \frac{1}{V}\left\{ \sum_{\text{i}} \vec{v}_{\text{i}} h_{\text{i}} + \sum_{i=1}^{N}\sum_{j=1, j\neq i}^{N}\left(\frac{1}{2}\vec{r}_{\text{ij}}\cdot(\vec{F}_{\text{ij}}\cdot\vec{v}) + \frac{1}{6}\sum_{k=1, k\neq i, j}^{N}(\vec{r}_{\text{ij}}+\vec{r}_{ik})\cdot(\vec{F}_{\text{ijk}}\cdot v_{\text{i}})\right)_{\text{i}}\right\}, \qquad (14)$$

where the force components on atom $i$ are defined as:

$$\vec{F}_{\text{ij}} = -\left.\frac{\partial V_{\text{ij}}}{\partial \vec{r}_{\text{i}}}\right|_{\text{r}_{\text{j}}, \text{j}\neq\text{i}} \quad \text{and} \quad \vec{F}_{\text{ijk}} = -\left.\frac{\partial V_{\text{ijk}}}{\partial \vec{r}_{\text{i}}}\right|_{\text{r}_{\text{j}}, \text{r}_{\text{k}}} \qquad (15)$$

and $\vec{v}_{\text{i}}$ and $\vec{r}_{\text{i}}$ are respectively the $i$-site velocity and position vectors, while $\vec{r}_{\text{ij}}$ is the $i$-$j$ sites relative position vector.

All molecular dynamics simulations in the present work are carried out using a fixed 1fs time increment. For each simulation run, the system is first equilibrated under an isothermal condition using the Berendsen thermostat [20] for 40 ps. Subsequently, constant energy molecular dynamics simulations are carried out for 400 ps. The atomic positions and velocities obtained at different simulation times are next used in conjunction with Equation 14 to calculate the heat flux at every time step. The heat-flux auto-correlation function is next computed as a function of the correlation time using Equation 8. Lastly, the lattice thermal conductivity is computed using Equation 4.

TABLE II Optical and acoustic weighting factors, $A_o$ and $A_a$, and relaxation times, $\tau_o$ and $\tau_a$, obtained by nonlinear least squares fitting of the heat current autocorrelation function for (10,10) armchair single-walled carbon nanotubes

| Numbers of atoms | Cell length (nm) | $A_o$ $10^{-6}$ $(\frac{J^2}{cms^2})$ | $\tau_o$ (ps) | $A_a$ $10^{-6}$ $(\frac{J^2}{cms^2})$ | $\tau_a$ (ps) | $\frac{A_0\tau_0}{A_0\tau_0+A_a\tau_a}$ |
|---|---|---|---|---|---|---|
| 400 | 2.477 | 3.339 | 0.074 | 1.211 | 17.597 | 0.0012 |
| 800 | 4.954 | 3.334 | 0.070 | 1.216 | 17.870 | 0.0011 |
| 1600 | 9.908 | 3.299 | 0.072 | 1.227 | 17.940 | 0.0011 |
| 3200 | 19.816 | 3.376 | 0.069 | 1.232 | 17.851 | 0.0011 |
| 6400 | 39.632 | 3.339 | 0.070 | 1.230 | 17.877 | 0.0011 |
| Average | | 3.343 | 0.070 | 1.229 | 17.869 | |

TABLE III Optical and acoustic weighting factors, $A_o$ and $A_a$, and relaxation times, $\tau_o$ and $\tau_a$, obtained by nonlinear least squares fitting of the heat current autocorrelation function for (18, 0) zig-zag single-walled carbon nanotubes

| Numbers of atoms | Cell length (nm) | $A_o$ $10^{-6}$ $(\frac{J^2}{cms^2})$ | $\tau_o$ (ps) | $A_a$ $10^{-6}$ $(\frac{J^2}{cms^2})$ | $\tau_a$ (ps) | $\frac{A_0\tau_0}{A_0\tau_0+A_a\tau_a}$ |
|---|---|---|---|---|---|---|
| 360 | 2.145 | 3.327 | 0.075 | 1.135 | 17.230 | 0.0013 |
| 720 | 4.290 | 3.329 | 0.071 | 1.141 | 17.306 | 0.0012 |
| 1440 | 8.580 | 3.338 | 0.073 | 1.150 | 17.395 | 0.0012 |
| 2880 | 17.160 | 3.330 | 0.071 | 1.153 | 17.349 | 0.0012 |
| 5760 | 34.320 | 3.344 | 0.069 | 1.150 | 17.401 | 0.0012 |
| Average | | 3.338 | 0.070 | 1.150 | 17.375 | |

TABLE IV Optical and acoustic weighting factors, $A_o$ and $A_a$, and relaxation times, $\tau_o$ and $\tau_a$, obtained by nonlinear least squares fitting of the heat current autocorrelation function for (14, 6) single-walled carbon nanotubes

| Numbers of atoms | Cell length (nm) | $A_o$ $10^{-6}$ $(\frac{J^2}{cms^2})$ | $\tau_o$ (ps) | $A_a$ $10^{-6}$ $(\frac{J^2}{cms^2})$ | $\tau_a$ (ps) | $\frac{A_0\tau_0}{A_0\tau_0+A_a\tau_a}$ |
|---|---|---|---|---|---|---|
| 632 | 3.813 | 3.280 | 0.068 | 1.129 | 16.774 | 0.0012 |
| 1264 | 7.626 | 3.294 | 0.070 | 1.133 | 16.803 | 0.0012 |
| 528 | 15.252 | 3.289 | 0.069 | 1.134 | 16.906 | 0.0012 |
| 5056 | 30.504 | 3.330 | 0.065 | 1.135 | 16.899 | 0.0011 |
| Average | | 3.311 | 0.069 | 1.131 | 16.880 | |

## 3. Results and discussion

### 3.1. The effect of computational cell size

As discussed earlier, the relative magnitudes of the computational cell size with respect to the phonon mean free path can be an important factor affecting the accuracy of thermal conductivity computed through the use of atomistic simulations. When the simulation cell is too small, the time for phonons to travel through the simulation cell and to reenter it on the other side of the cell is shorter than the decay time of the heat-flux auto-correlation function. This causes phonon scattering to take place more frequently than it would in an infinite crystal. Consequently, only the auto-correlation functions at short correlation times are expected to be accurate. Nevertheless, Che *et al*. [2] showed that thermal conductivity can be computed using computational cells significantly smaller than the phonon mean free path. Using the macroscopic laws of relaxation and the Onsager's postulate for microscopic thermal fluctuations, Che *et al*. [2] first showed that the long-time (acoustic phonons controlled) asymptotic decay of the heat-flux auto-correlation function (which makes the dominant contribution to the thermal conductivity) is of an exponential type. Consequently, relatively short-time simulation-based heat-flux auto-correlation data obtained in medium-size computational cells can be used to determine quite accurately the exponential decay parameters of the heat-flux auto-correlation function.

To determine the effect of the computational cell size on the lattice contribution to thermal conductivity, five different sizes of the computational cell are used in the present work for each of the three selected carbon nanotubes. The number of atoms in the computational cell in each case is given in Tables II–IV. Since the single walled carbon nanotubes are one atomic layer thick, only the thermal conductivity in the direction of the nanotubes axis is computed. This is achieved by using only the data for heat flux in the direction of nanotubes axis when calculating the corresponding auto-correlation functions via Equation 5.

Examples of typical heat-current auto-correlation functions for the (10, 10), (18, 0) and (14, 6) nanotubes obtained in the present work are shown in Fig. 2a–c, respectively. These functions are obtained using computational cells containing 3200, 2880 and 2528 atoms, respectively. In general, the auto-correlation functions are characterized by a rapid initial decay followed by a gradual, long-time exponential decay. The initial fast decay can be attributed to the high-frequency optical phonon modes which are associated with out-of-phase vibrations of the atoms residing on two sublattices in the two-dimensional hexagonal nanotube crystal structure. These phonons are generally scarcely

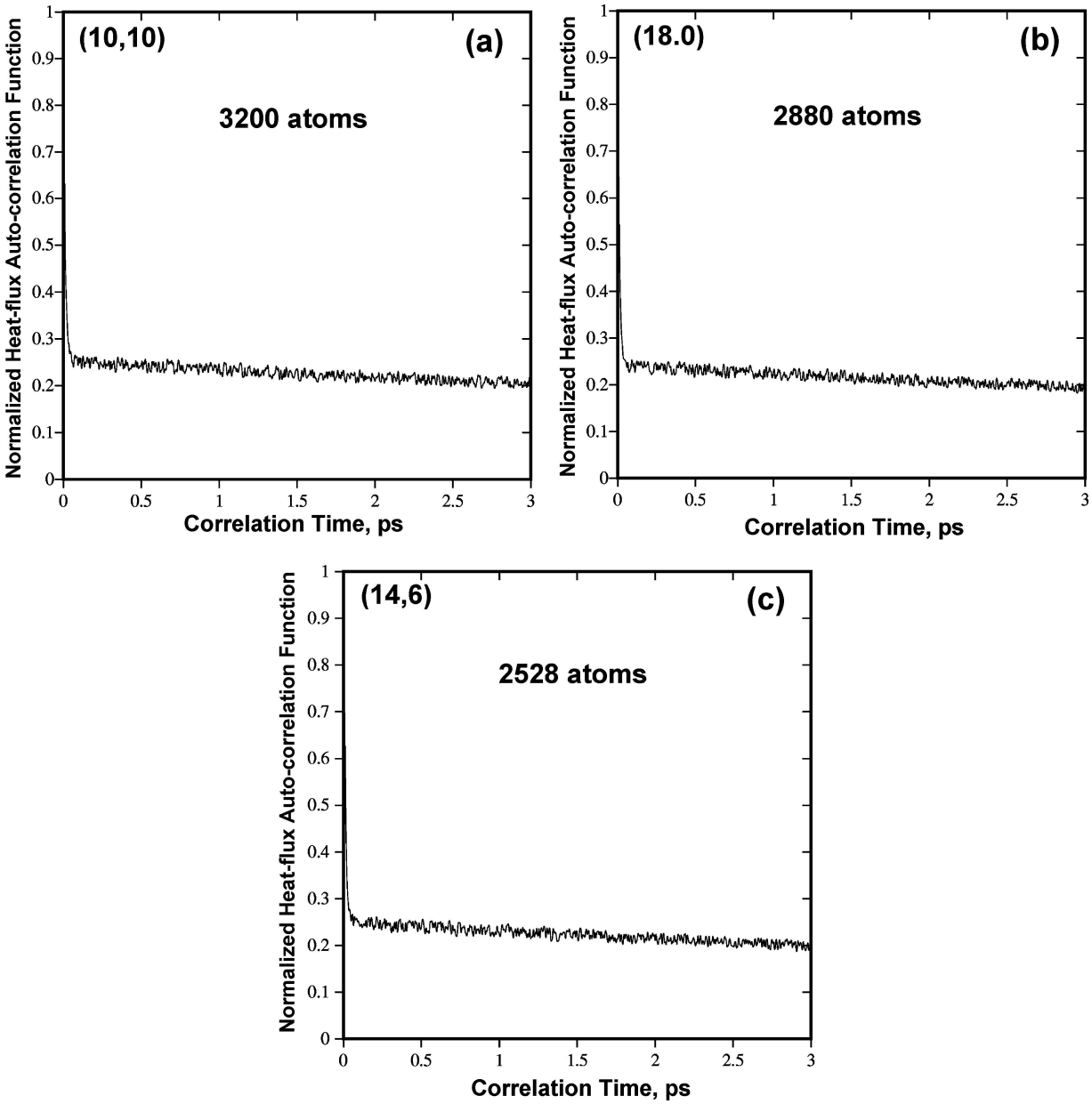


*Figure 2* Heat-current auto-correlation functions for: (a) a (10, 10); (b) a (18, 0) and (c) a (14, 6) single-walled carbon nanotube at 300 K.

populated and weakly coupled with low-frequency (in-phase vibration) acoustic modes at room temperature and, hence, they do not significantly contribute to thermal conductivity. The long-time behavior of the heat-current auto-correlation functions and, hence, thermal conductivity is controlled by low-frequency acoustic phonon modes.

The auto-correlation function results such as the one shown in Fig. 2a–c are fitted using the Levenberg-Marquardt nonlinear least-squares method [21] to the following double exponential function:

$$C_{\mathrm{J}}^{\mathrm{C}}(t) = A_0 \exp(-t/\tau_{\mathrm{o}}) + A_{\mathrm{a}} \exp(-t/\tau_{\mathrm{a}}), \quad t \geq 0, \quad (16)$$

where the subscript *o* and *a* are used to denote the optical and acoustic phonon modes, respectively. Substitution of Equation 16 in Equation 4 yields the following expression for the thermal conductivity:

$$\Lambda^{\mathrm{C}} = \frac{V}{k_{\mathrm{B}} T^2}(A_{\mathrm{o}}\tau_{\mathrm{o}} + A_{\mathrm{a}}\tau_{\mathrm{a}}). \quad (17)$$

Following the procedure suggested by Che *et al.* [2], the heat-flux auto-correlation function results for all simulation runs corresponding to the first 3 ps of the correlation time are fitted to the function defined in Equation 16 to determine the parameters $A_{\mathrm{o}}$, $\tau_{\mathrm{o}}$, $A_{\mathrm{a}}$, and $\tau_{\mathrm{a}}$. The results of this procedure are given in Tables II–IV. A simple analysis of the results shown in Tables II–IV indicates that the contribution of the high-frequency optical phonon modes to the thermal conductivity, $(A_{\mathrm{o}}\tau_{\mathrm{o}}) / (A_{\mathrm{o}}\tau_{\mathrm{o}} + A_a\tau_a)$, is indeed very small and is typically on the order of 0.1%.

The values of the weighting factors $A_{\mathrm{o}}$ and $A_{\mathrm{a}}$ and the corresponding exponential decay constants $\tau_{\mathrm{o}}$ and $\tau_{\mathrm{a}}$ obtained by the nonlinear least-squares fitting of the heat-flux auto-correlation functions in the three types

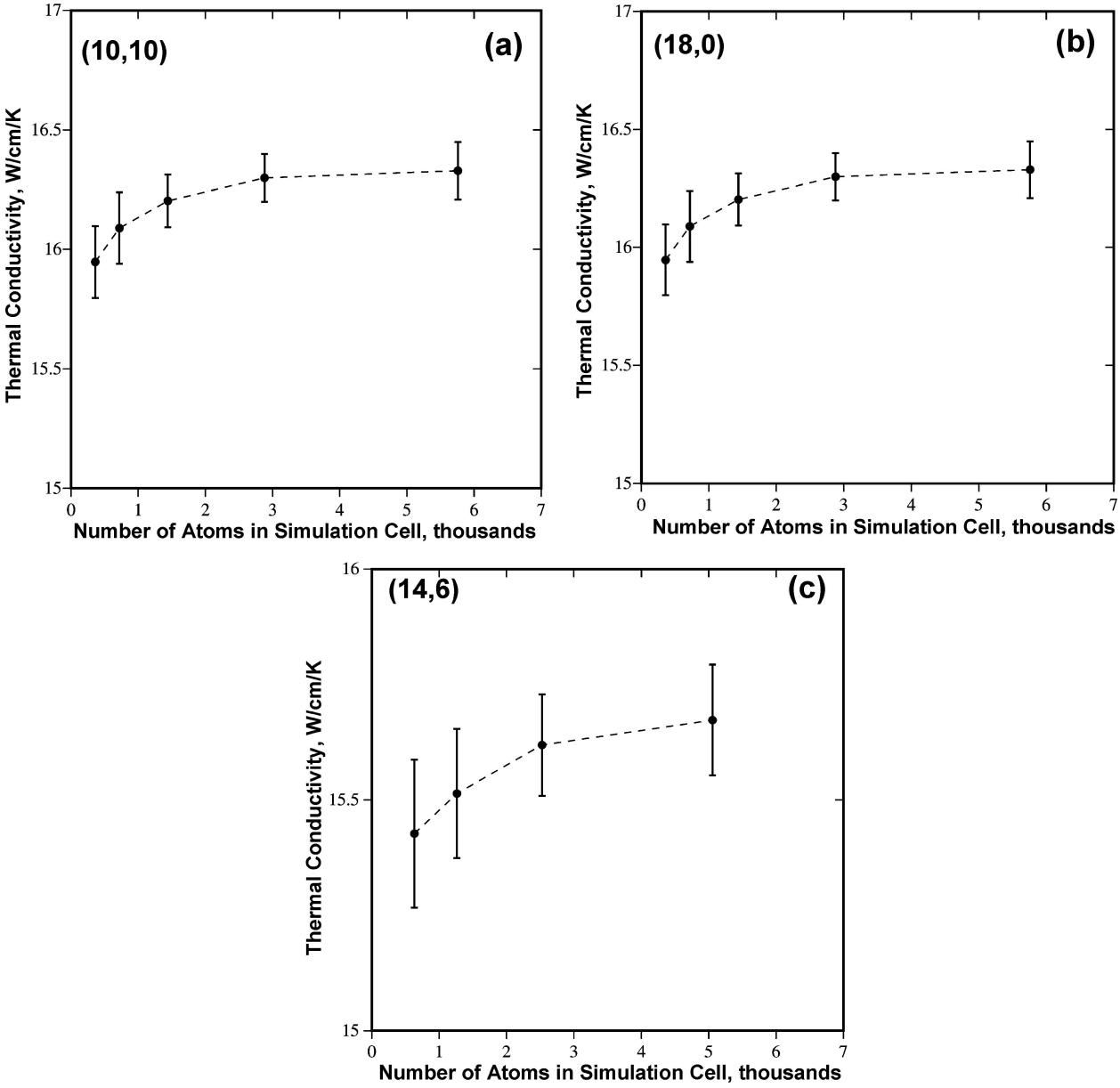


*Figure 3* Lattice thermal conductivity in: (a) a (10, 10); (b) a (18, 0) and (c) a (14, 6) single-walled carbon nanotube at 300 K.

of nanotubes and for the simulation cells with different numbers of atoms are listed in Table II–IV. To determine the average values of these parameters, the weighting factors $A_o$ and $A_a$ are normalized by the nanotube volume, weighted by the number of atoms in each simulation and averaged over all simulations for a given type of nanotube. Similar averaging without volume normalization is used to obtain average values for the relaxation times, $\tau_o$ and $\tau_a$. The results of this procedure are listed in Tables II–IV in the row denoted as "*average*".

The dependence of thermal conductivity on the size of the simulation cell for the three types of carbon nanotubes analyzed in the present work is displayed in Fig. 3a–c. The error bars shown in Fig. 3a–b correspond to $\pm$ one standard deviation for the results of five molecular dynamics runs. The results displayed in Fig. 3a–c show that, as expected, when the simulation cell is too small (i.e., contains less than $\sim$1000 atoms), the atoms in a region of the simulation cell do not have enough time to lose their previous dynamic information before a periodically equivalent phonon (i.e., the same phonon which reentered the cell at the opposite boundary) arrives in this region. Consequently, the corresponding correlation functions are contaminated by such "*memory*" effects and they do not reflect the dynamic behavior encountered in a real system and the computed thermal conductivity is not very accurate. On the other hand, when the computational cell size is increased, the memory effects become less pronounced and the computed thermal conductivity is more accurate. The results displayed in Fig. 3a–c show that at larger cell sizes thermal conductivity becomes apparently independent (or very weakly dependent) of the size of the computational cell. The results shown in Fig. 3a–c further suggest that there is a minimum "critical" size of the computational cell beyond which the memory effects practically do not affect the thermal conductivity. In the case of the maximum correlation time of 3 ps, the minimum cell size is approximately 15–20 nm and such cells contain on the order of 3000–3500 atoms.

The analysis presented above established a minimum critical computation cell size beyond which the cell size does not apparently affect the thermal conductivity. It is important to determine how the critical cell size compares with the phonon mean free path in single-walled carbon nanotubes. To estimate the phonon mean free path, $L$, the following relation for the thermal conductivity from the kinetic theory of solids is used [22]:

$$\Lambda \approx \frac{1}{3} C_{\mathrm{v}} \rho v L \tag{18}$$

where $C_{\mathrm{v}}$ is the mass-based constant-volume specific heat and $v$ is the speed of sound. The molecular dynamics simulations carried out in the present work yielded the mean interatomic spacing of 0.142 nm. The density of single-walled carbon nanotubes is difficult to determine since they are one-atom thick. Since the single-walled carbon nanotubes are typically found bundled in ropes with a one-dimensional triangular arrangement and an inter-tube spacing equal to the Van der Walls radius of carbon (0.17 nm), the nanotubes' wall thickness is set equal to this value. This procedure yielded the density of $\rho = 2.3$ g/cm$^3$. This value is very close to the bulk density of graphite. The experimental values for the specific heat of $C_{\mathrm{v}} = 500$ J/kg/K and for compressibility of $\beta_{\mathrm{T}} = 0.024$ GPa$^{-1}$ for single-walled carbon nanotubes of comparable diameters has been taken from Refs. [23] and [24]. Using the following equation: $v = 1/\sqrt{\rho \beta_{\mathrm{T}}}$, the speed of sound has been computed as 4,256 m/s. Lastly, using the average thermal conductivity for the three types of nanotubes, $\Lambda = 16.5$ W/cm/K, and Equation 18, the mean free path for acoustic phonons of $L \approx 1{,}000$ nm has been obtained. Thus, the acoustic phonon mean free path is larger than the critical computational cell size by a factor of 50–65.

The finding presented above shows that despite the fact that the phonon mean free path is considerably larger than the sizes of the computational cells used, an apparent convergence in the thermal conductivity can be obtained, Fig. 3a–c. It should be noted that in order to set the computational cell size comparable with the phonon mean free path, computational cells containing on the order of $10^7$–$10^8$ atoms would have to be used. Molecular dynamics simulations involving such a large number of atoms, while feasible (particularly if an advantage is taken of the parallel computing), would be computational very expensive and are not very appealing. Instead, as initially suggested by Che *et al*. [2] and also reaffirmed in our prior work [14], smaller size simulation cells and short-time heat-flux auto-correlation functions can be used to quantify the thermal conductivity. This suggestion is challenged in the present work through the use of a spectral Green-Kubo relation, as discussed in the next section.

## 3.2. Wavelength cut-off correction of the thermal conductivity

The results displayed in Fig. 3a–c and discussed in the previous section suggest that the artifacts associated with reentering phonons in the computational cells of a finite size can be practically eliminated using the cell sizes which are 50–60 times smaller than the phonon mean free path. However, there are additional potential artifacts associated with the use of computational cells of a finite size which need to be addressed. The potential artifact analyzed in this section is associated with the fact that in molecular dynamics simulations only the phonons with a wavelength shorter than or equal to the computational cell size are permitted. Due to such a wavelength cut-off, the contribution of the long-wavelength (i.e., low-frequency) phonons to the thermal conductivity is not accounted for. The long-wavelength phonons are generally associated with the largest group velocity and, in accordance with Equation 18, (in which the sound velocity is replaced with the group velocity), make the largest contribution to the thermal conductivity. Thus, despite the apparent convergence of the thermal conductivity at larger computational cell sizes in Fig. 3(a)–(c), one may expect that the computed thermal conductivities are underpredicted since the contribution of the long-wavelength phonons is not accounted for.

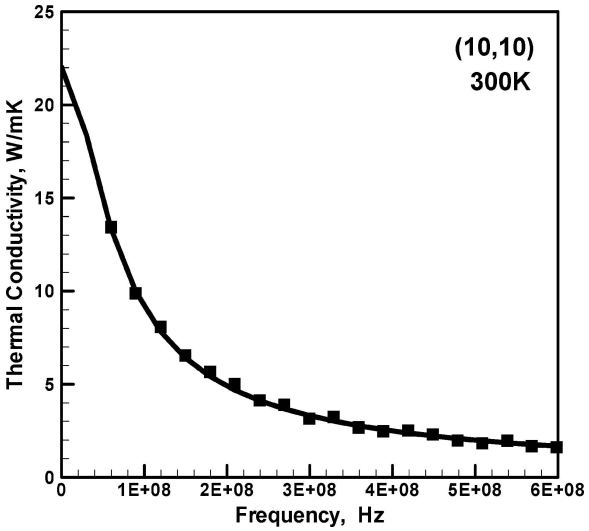


*Figure 4* Magnitude of the spectral thermal conductivity in a (10, 10) single-walled carbon nanotube at 300 K as a function of the frequency.

To correct the values of the thermal conductivity obtained in the previous section in order to include the contribution of the long-wavelength phonons, the procedure proposed by Volz and Chen [25, 26] is followed in the present work. Within this procedure, a complex, frequency-dependent thermal conductivity, $\Lambda^{\mathrm{C}}(\omega)$, is first defined using the spectral Green-Kubo relation as:

$$\Lambda^{\mathrm{C}}(\omega) = \frac{V}{k_{\mathrm{B}} T^2} \int_0^{\infty} \langle \vec{J}_{\mathrm{q}}(0) \cdot \vec{J}_{\mathrm{q}}(t) \rangle e^{\mathrm{i}\omega t} \, \mathrm{d}t \tag{19}$$

where $\omega$ is the angular frequency.

Next the magnitude of the complex thermal conductivity is defined within a phonon relaxation time approximation as:

$$|\Lambda(\omega)| = V \langle \vec{J}_{\mathrm{q}}(0)^2 \rangle / [k_B T^2 \sqrt{\omega^2 + \tau^{-2}}] \tag{20}$$

where $\tau$ is the average phonon relaxation time.

The heat-flux auto-correlation functions defined in Section 3.1 are then substituted in Equation 19, and the resulting equation integrated analytically for the magnitude of the complex thermal conductivity. In these calculation a minimum cut-off frequency $\omega_{\text{cut-off}} = 5 \cdot 10^{-4}$ THz was used which corresponds to an average wavelength of the permitted phonons of 20 nm. An example of the results of this procedure is displayed as filled circles in Fig. 4.

Next, the filled-circle data displayed in Fig. 4 are fitted to the relation given by Equation 20 using the Levenberg–Marquardt least-squares procedure [21]. The results of the fitting procedure are shown as a solid line in Fig. 4. The fitting line is extrapolated to the zero value of frequency in order to compute the static thermal conductivity, i.e., the thermal conductivity associated with the phonons with an infinite wavelength which, as discussed earlier, make the dominant contribution to the thermal conduction.

The static value of the thermal conductivity computed using the results displayed in Fig. 4, $\Lambda^C = 22.0$ W/cm · K is larger than its counterpart obtained in Section 3.1 ($\Lambda^C = 17.9$ W/cm · K) by about 23 percent. Similar results are obtained in the case of other two carbon nanotubes. This finding suggests that the contribution of the long-wavelength phonons (which are not permitted within molecular dynamics simulations based on the computational cell of a finite size) is indeed significant and has to be taken into account.

## 3.3. The effect of chirality

The results displayed in Fig. 3a–c further show that chirality has an effect on the lattice part of thermal conductivity in single-walled carbon nanotubes. Specifically, thermal conductivity is the highest ($\lambda$=17.8 W/cm/K) in the (10, 10) arm-chair nanotube and the lowest ($\lambda$=15.6 W/cm/K) in the (14, 6) nanotube of general chirality. Since these results pertain to the lattice contribution to thermal conductivity alone, they have to be attributed to differences in phonon-phonon interactions and the resulting differences in mean free path in the three types of nanotubes. As stated earlier, a detailed modeling of phonon–phonon interactions is very complicated [13] and it is beyond the scope of the present study. Nevertheless, it is well established that lattice thermal conductivity is controlled by the momentum conservation of the so-called "*Umklapp*" phonon collisions represented as: $k_1 + k_2 = k_3 + G$, where $k_1$ and $k_2$ are wave vectors of the colliding phonons, $k_3$ the wave vector of the resulting phonon and $G$ is $2\pi$ times a reciprocal lattice vector. Due to the differences in chirality and the resulting differences in magnitudes of the periodic lengths in the axial direction, one could expect similar differences in the permissible $G$ vectors and, hence, in the lattice thermal conductivity in the three nanotubes analyzed.

It should be noted that, based on the magnitude of the band gap alone, the electronic contribution to the thermal conductivity can also be expected to be the highest in the metallic-type (10, 10) nanotube and the lowest in the semiconductor like (14, 6) nanotube. It should be noted, however, that in addition to the band gap, the electronic band structure as well as electron-electron and electron-phonon scattering also affect the electronic contribution to the thermal conductivity. Nevertheless, the observation that the lattice thermal conductivity can vary by as much as 20% with nanotube chirality and that the electronic thermal conductivity can be affected in the same direction by chirality, suggests that the thermal conductivity of individual single-walled nanotubes in nanotube ropes (consist of nanotubes of various chirality) can vary substantially from one nanotube to the other.

## 3.4. The effect of temperature

The molecular-dynamics spectral Green-Kubo relation based procedure for computation of the static thermal conductivity in the three types of single-walled carbon nanotubes described in Sections 3.2 is utilized in this section to quantify the temperature dependence of the thermal conductivity in these materials. Over the last few years, there has been a number of experimental and theoretical investigations of the effect of temperature on the thermal conductivity in single-walled carbon nanotube bundles and of individual multi-walled carbon nanotubes [24, 27–30]. However, due to serious experimental challenges discussed earlier, no reliable experimental data presently exist for the thermal conductivity of individual single-walled carbon nanotubes.

The effect of temperature in a range between 50 and 400 K on the mean value of the thermal conductivity in the three types on single-walled carbon nanotubes analyzed in the present work is shown in Fig. 5. The results displayed in Fig. 5, showed that at the lowest temperature explored, the thermal conductivity increases with an increase in temperature while in the upper portion of the temperature range examined, the thermal conductivity decreases with an increase in temperature. This finding suggests that, at low temperatures, the thermal conductivity is dominated by the drift of acoustic phonons whose number increases with temperature while, at high temperatures, phonon-phonon "*Umklapp*" scattering which hinders

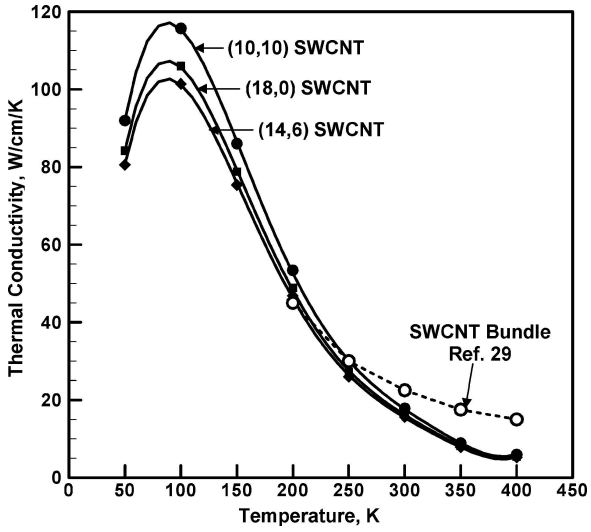


*Figure 5* The effect of temperature on the thermal conductivity in the three types of single-walled carbon nanotubes analyzed in the present work.

heat transfer causes the thermal conductivity to decrease with an increase in temperature [25].

For comparison, experimental results pertaining to the effect of temperature on the thermal conductivity in a bundle of the single-walled carbon nanotubes are also displayed in Fig. 5 [27]. While the agreement between the computational and the experimental results in the common temperature range can be characterized as only fair, the true validation of the present computational model entails the availability of experimental thermal conductivities for the isolated single-walled carbon nanotubes with a known chirality. Unfortunately, as stated earlier, such experimental thermal conductivity data are presently not available.

## 4. Conclusions

Based on the results obtained in the present work, the following main conclusions can be drawn:

1. By fitting the long-time molecular-dynamics based heat-flux auto-correlation functions to a double-exponential decay relation, the artifacts associated with reentering phonons in the computational cells smaller than the phonon mean free path can be practically eliminated when computing the lattice contribution to the thermal conductivity in single-walled carbon nanotubes.

2. However, to account for the contribution of long-wavelength phonons (not permitted in the computational cells of a finite size) to the thermal conductivity, a procedure based on the spectral Green-Kubo relation from the linear response theory is found to be very instrumental.

3. The lattice contribution to the thermal conductivity can vary by as much as 20% in single-walled carbon nanotubes with a nearly equivalent radius depending on their chirality.

4. The molecular dynamics based procedure for computation of the thermal conductivity presented in the present work clearly shows the competition between two opposing phenomena during an increase in temperature: (a) an increase in the thermal conductivity due to an increase in the phonon occupation number and (b) a decrease in the thermal conductivity due to a ever more pronounced "*Umklapp*" phonon scattering.

5. The method presented is not limited to carbon nanotubes and can be readily extended to other types of nanotubes such as boron nitride and vanadium oxide nanotubes.


## Acknowledgements

The material presented in this paper is based on work supported by the U.S. Army Grant Number DAAD19-01-1-0661. The authors are indebted to Drs., Fred Stenton and William DeRosset of ARL for the support and a continuing interest in the present work.


## References


1. P. STACHOWIAK, V. V. SUMAROKOV, J. MUCHA and A. JEZOWSKI, *Phys. Rev. B* **58** (1998) 2380.
2. J. CHE, T. CAGIN, W. DENG and W. A. GODDARD III, *J. Chem. Phys.* **113** (2000) 6888.
3. L. CHICO, V. H. CRESPI and L. X. BENEDICT, *Phys. Rev. Lett.* **76** (1996) 971.
4. L. LANGER, V. BAYOT and E. GRIVEI, *ibid.* **76** (1996) 479.
5. T. W. EBBESEN, H. J. LEZEC, H. HIURA, J. W. BENNETT, H. F. GHAEMI and T. THIO, *Nature* **382** (1996) 54.
6. T. PICHLER, M. KNUPFER and M. S. GOLDEN, *Phys. Rev. Lett.* **80** (1998) 4729.
7. D. J. EVANS, *Phys. Lett.* **91A** (1982) 457.
8. D. MACGOWAN and D. J. EVANS, *ibid.* **A 117** (1986) 414.
9. P. J. DAVIS and D. J. EVANS, *J. Chem. Phys.* **103** (1995) 4261.
10. S. WALKAUSKAS, D. BROIDO, K KEMPA and T. REINECKE, *J. Appl. Phys.* **85** (1999) 2579.
11. A. BALANDIN and K. WANG, *Phys. Rev. B* **58** (1998) 1544.
12. V. L. GUREVICH, "Transport in Phonon Systems" (North-Holland, Amsterdam, 1986).
13. M. J. GILLAN, *Phys. Scr., T* **T39** (1991) 362.
14. M. GRUJICIC, G. CAO and B. GERSTEN, *Mater. Sci. Engng.* **B107** (2004) 204.
15. G. D. MAHAN, "Many-Particle Physics" (Plenum, New York, 1993).
16. R. KUBO, M. TODA and N. HASHITSUME, "Statistical Physics" (Springer, Berlin, 1985) Vol. II.
17. G. D. MAHAN, "Many-Particle Physics" (Plenum, New York, 1993).
18. S. J. STUART, A. B. TUTEIN and J. A. HARRISON, *J. Chem. Phys.* **112** (2000) 6472.
19. D. W. BRENNER, S. B. SINNOTT and J. A. HARRISON (unpublished).
20. H. J. C. BERENDSEN, J. P. M. POSTMA, W. F. VAN GUNSTEREN, A. DI NOLA and J. R. HAAK, *J. Chem. Phys.* **81** (1984) 3684.
21. W. H. PRESS, B. P. FLANNERY, S. A. TEUKOLSKY and W. P. VETTERLING, "Numerical Recipes: The Art of Scientific Computing" (Cambridge University Press, 1986).
22. J. M. ZIMAN, "Principles of the Theory of Solids" (Cambridge University Press, Cambridge, 1972).
23. W. YI, L. LU, D.-L. ZHANG, Z. W. PAN and S. S. XIE, *Phys. Rev. B* **59** (1999) R9015.
24. J. TANG, L.-C. QIN, T. SASAKI, M. YUDASAKA, A. MATSUSHITA and S. IIJIMA, *Phys. Rev. Lett.* **85** (2000) 1887.
25. S. G. VOLZ and G. CHEN, *Phys. Rev. B* **61** (2000) 2651.
26. *Idem.*, *Physica B* **263–264** (1999) 709.
27. J. HONE, M. WHITNEY, C. PISKOTI and A. ZETTL, *Phys. Rev. B* **59** (1999) R2541.
28. P. KIM, L. SHI, A. MAJUMDAR and P. L. McEUEN, *Phys. Rev. Lett.* **87** (2001) 215502.
29. S. BERBER, Y. K. KWON and D. TOMANEK, *ibid.* **84** (2000) 4613.
30. B. A. GLAVIN, *ibid.* **86** (2001) 4318.



*Received 17 September*
*and accepted 9 December 2004*